Journal of Geophysical Research: Atmospheres

Supporting information for

Observational constraints on glyoxal production from isoprene oxidation and its contribution to organic aerosol over the Southeastern United States

Jingyi Li[1], Jingqiu Mao[1,2] , Kyung-Eun Min[3,4,5], Rebecca A. Washenfelder[3,4], Steven S. Brown[3,6], Jennifer Kaiser[7], Frank N. Keutsch[8], Rainer Volkamer[4,6], Glenn M. Wolfe[9,10], Thomas F. Hanisco[10], Ilana B. Pollack[3,4,11], Thomas B. Ryerson[3], Martin Graus[3,4,12], Jessica B. Gilman[3,4], Brian M. Lerner[3,4], Carsten Warneke[3,4], Joost A. de Gouw[3,4], Ann M. Middlebrook[3], Jin Liao[3,4], André Welti[3,4,13], Barron H. Henderson[14], V. Faye McNeill[15], Samuel R. Hall[16], Kirk Ullmann[16], Leo J. Donner[2], Fabien Paulot[1,2], and Larry W. Horowitz[2]

[1]Program in Atmospheric and Oceanic Sciences, Princeton University, Princeton, New Jersey, USA
[2]Geophysical Fluid Dynamics Laboratory, National Oceanic and Atmospheric Administration, Princeton, New Jersey, USA
[3]Chemical Sciences Division, NOAA Earth System Research Laboratory, Boulder, Colorado, USA
[4]Cooperative Institute for Research in Environmental Sciences, University of Colorado, Boulder, Colorado, USA
[5]Now at School of Environmental Science and Engineering, Gwangju Institute of Science and Technology, Gwangju, Korea
[6]Department of Chemistry and Biochemistry, University of Colorado, Boulder, Colorado, USA
[7]School of Engineering and Applied Sciences, Harvard University, Cambridge, Massachusetts, USA
[8]School of Engineering and Applied Sciences and Department of Chemistry and Chemical Biology, Harvard University, Cambridge, Massachusetts, USA
[9]Joint Center for Earth Systems Technology, University of Maryland Baltimore County, Baltimore, Maryland, USA
[10]Atmospheric Chemistry and Dynamics Laboratory, NASA Goddard Space Flight Center, Greenbelt, Maryland, USA
[11]Now at Department of Atmospheric Science, Colorado State University, Fort Collins, Colorado, USA
[12]Now at Institute of Atmospheric and Cryospheric Sciences, University of Innsbruck, Innsbruck, Austria
[13]Now at Leibniz Institute for Tropospheric Research, Leipzig, Germany
[14]Department of Environmental Engineering Sciences, Engineering School of Sustainable Infrastructure and Environment, University of Florida, Gainesville, Florida, USA
[15]Department of Chemical Engineering, Columbia University, New York, New York, USA
[16]Atmospheric Chemistry Observations and Modeling Laboratory, National Center for Atmospheric Research, Boulder, Colorado, USA

Corresponding author: Jingqiu Mao (Jingqiu.Mao@noaa.gov)

Contents of this file

Text S1
Figures S1 to S8
Tables S1 to S2

Introduction

Supporting information consists of text, eight figures, and two tables:

- Text S1: Model sensitivity to heterogeneous loss of IEPOX
- Figure S1: Schematic of glyoxal production from isoprene oxidation by OH in AM3ST and AM3B.
- Figure S2: Box model-simulated cumulative yields of glyoxal and HCHO from isoprene
- Figure S3: Glyoxal along WP-3D aircraft during SENEX.
- Figure S4: Vertical profile of OH.
- Figure S5: Vertical profiles of photolysis rate of O_3 and NO_2.
- Figure S6: Vertical profiles of glyoxal from AM3ST and AM3B with different effective reactive uptake coefficients.
- Figure S7: Monthly averaged glyoxal, glyoxal SOA, ratio of glyoxal SOA to total SOA, and ratio of glyoxal SOA to total organic aerosol predicted by AM3ST below 1.5 km.
- Figure S8: Sensitivity of estimated glyoxal to heterogeneous loss of IEPOX.
- Table S1: Reaction rates of glyoxal and HCHO in AM3 and MCM v3.3.1 mechanisms.
- Table S2: Statistical analysis of model-measurement agreement for glyoxal below 1.5 km in model configurations with different effective reactive uptake coefficients.

Text S1. Model Sensitivity to heterogeneous loss of IEPOX

In the current work, heterogeneous loss of IEPOX to aerosols and clouds are not considered due to the high uncertainties in the loss rate. To examine the impact of heterogeneous loss of IEPOX on glyoxal yield, we did a series of sensitivity tests by assuming irreversible reactive uptake of IEPOX onto aerosols with an effective uptake coefficient γ of 1.0×10^{-4} and 1.0×10^{-3}. 1.0×10^{-4} is the value of γ on ammonium sulfate observed in chamber experiments [*Gaston et al.*, 2014]. 1.0×10^{-3} is the value of γ over the Southeast U.S. estimated by the CMAQ model [*Pye et al.*, 2013]. Absolute (base case – sensitivity case) and relative differences ((base case – sensitivity case)/base case) of modeled glyoxal are shown in Figure S8. We see that the impact on glyoxal estimate is not significant, about less than 15% of reduction in this region.

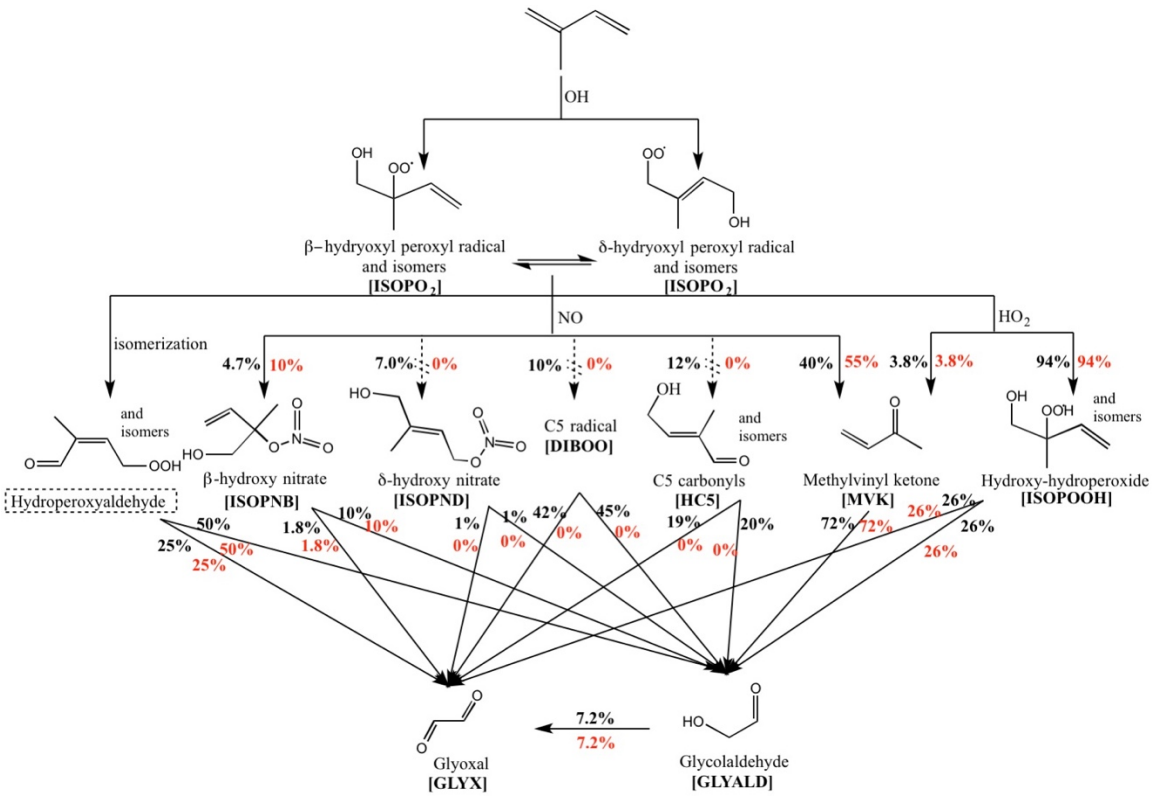

Figure S1. Schematic of glyoxal production from isoprene oxidation by OH in the AM3 mechanisms. Pathways represented in the dashed lines are removed in AM3B. The molar yields, shown in percentages, are for AM3ST (black) and AM3B (red) respectively. Species names in parentheses are that used in the model. The branching ratios for hydroxyl nitrates, DIBOO, HC5, MVK and ISOPOOH are calculated assuming $[O_3]$ = 60 ppbv; [OH] = 2.4×10^6 molecule cm^{-3}; and surface photolysis rates at 35°N latitude 12:00 LT on 1 June under clear-sky conditions. The peroxy radicals other than β- and δ-$ISOPO_2$ are assumed to react with NO only in the molar yield calculation. Hydroperoxyaldehyde, the product from isomerization of $ISOPO_2$ that generates glyoxal and glycolaldehyde via rapid photolysis, is ignored in the AM3 mechanisms.

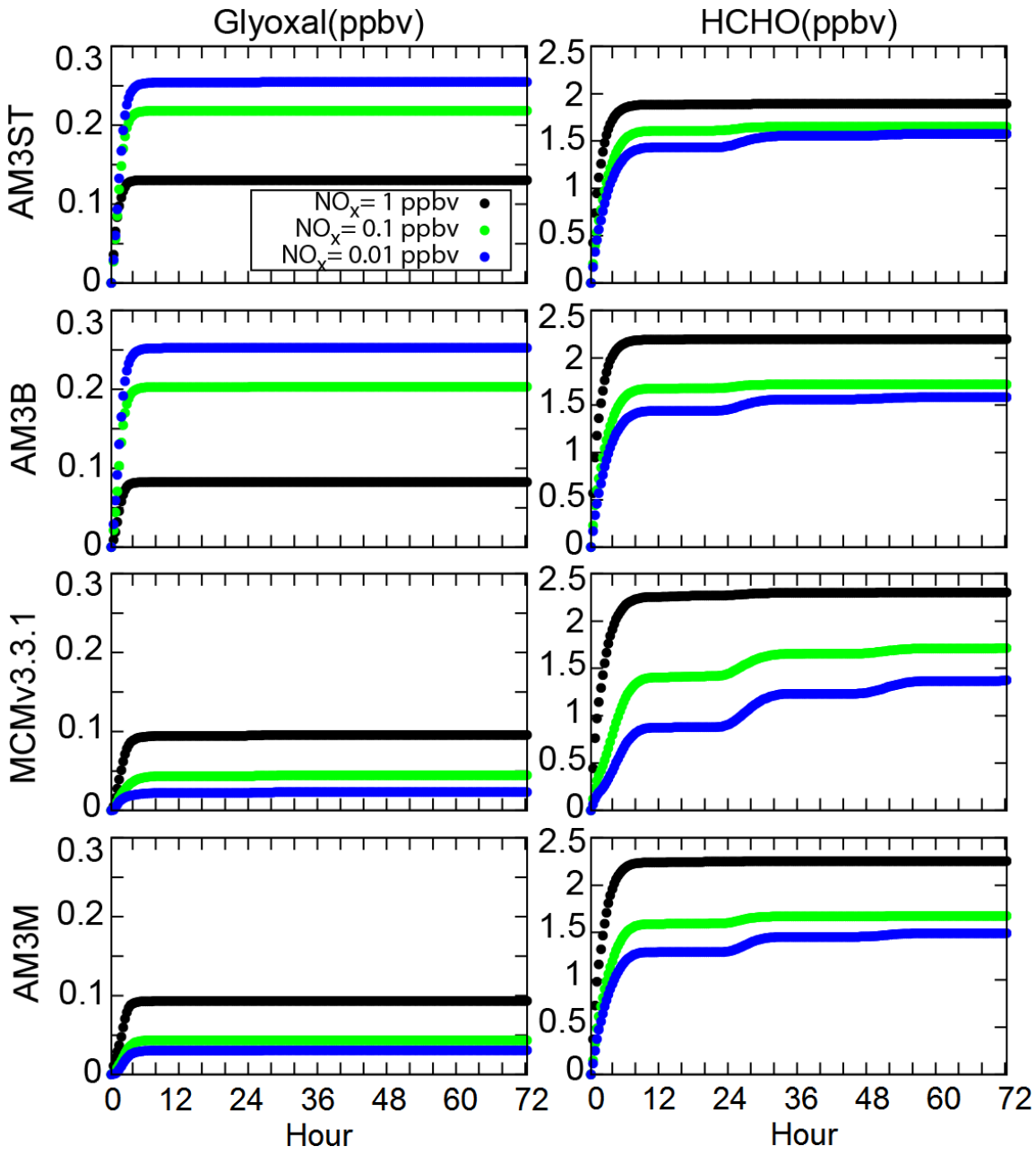

Figure S2. Box model-simulated cumulative yields of glyoxal and HCHO from isoprene. For each simulation, initial isoprene, ozone and CO are 1 ppbv, 60 ppbv, and 150 ppbv respectively; NO_x is constrained; temperature, pressure and relative humidity are held at 298K, 996hPa, and 80% respectively; the start time is 8:00 LT at 35°N latitude, on 1 June with diurnal variation of zenith angle (13.1° at noon) under clear-sky conditions. Glyoxal loss was neglected in the glyoxal simulations and HCHO loss was neglected in the HCHO simulations.

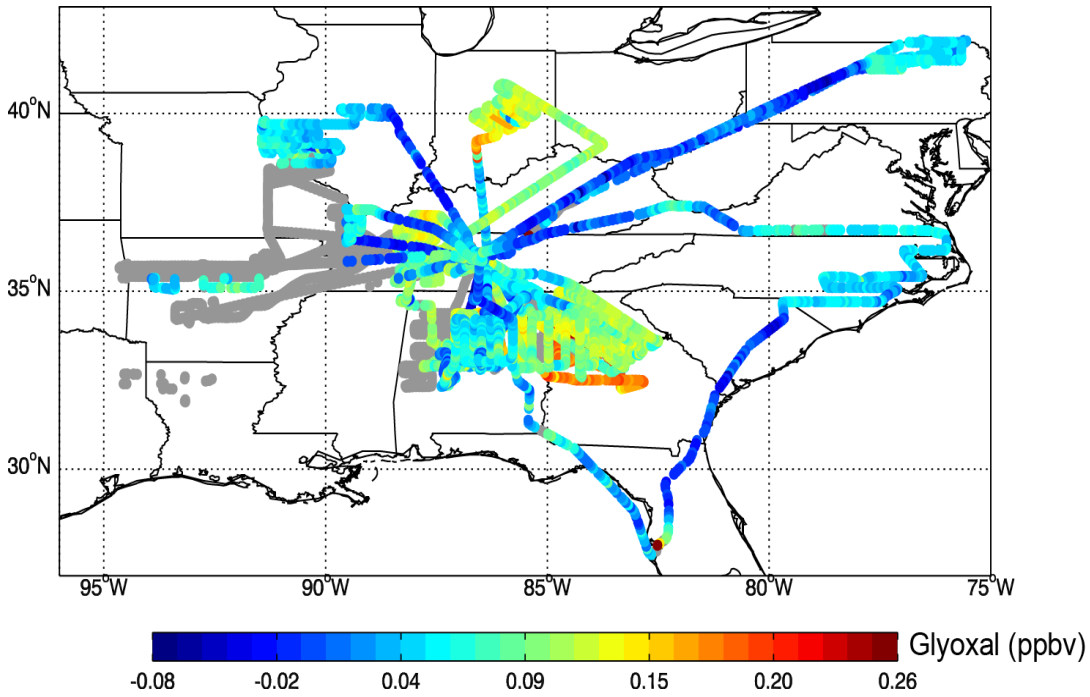

Figure S3. Glyoxal (ppbv) along WP-3D aircraft during SENEX. Grey colored data are from biomass burning, urban plumes, stratospheric air, the Ozark Mountains and nighttime flights.

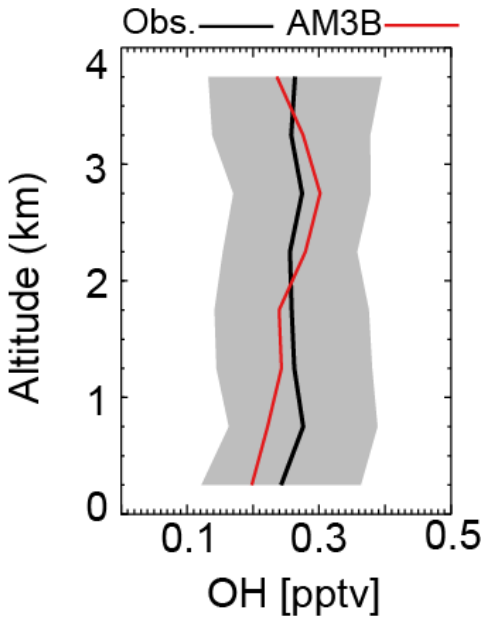

Figure S4. Mean vertical profile of OH from AM3B and observations during ICARTT.

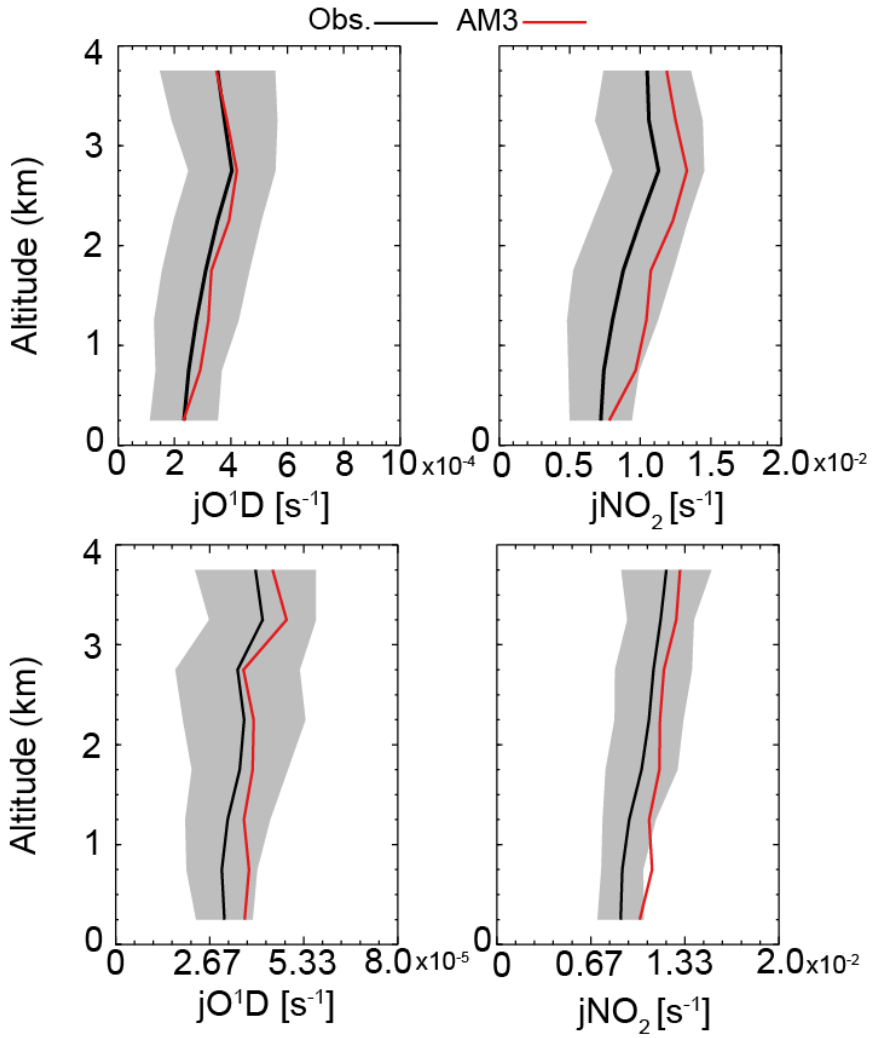

Figure S5. Mean vertical profiles of photolysis rate of O_3 (jO^1D) and NO_2 (jNO_2) from AM3 and observations during ICARTT (top row) and NOMADSS (bottom row)

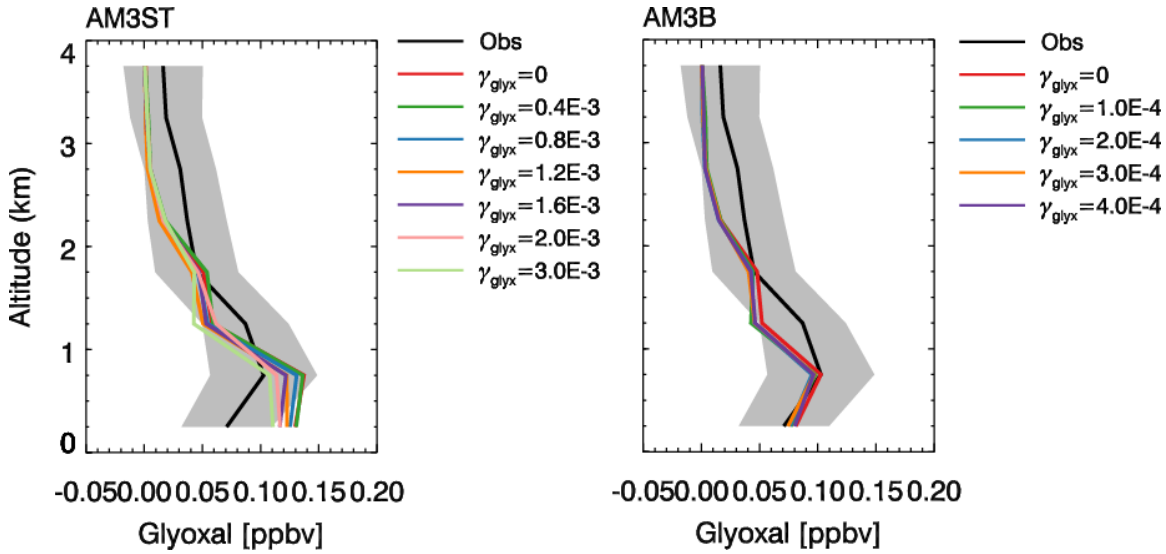

Figure S6. Vertical profiles of glyoxal from AM3ST (left) and AM3B (right) with different effective reactive uptake coefficients. The optimized γ_{glyx} that estimates the best fit to the observations is 2.0×10^{-3} for AM3ST and zero for AM3B.

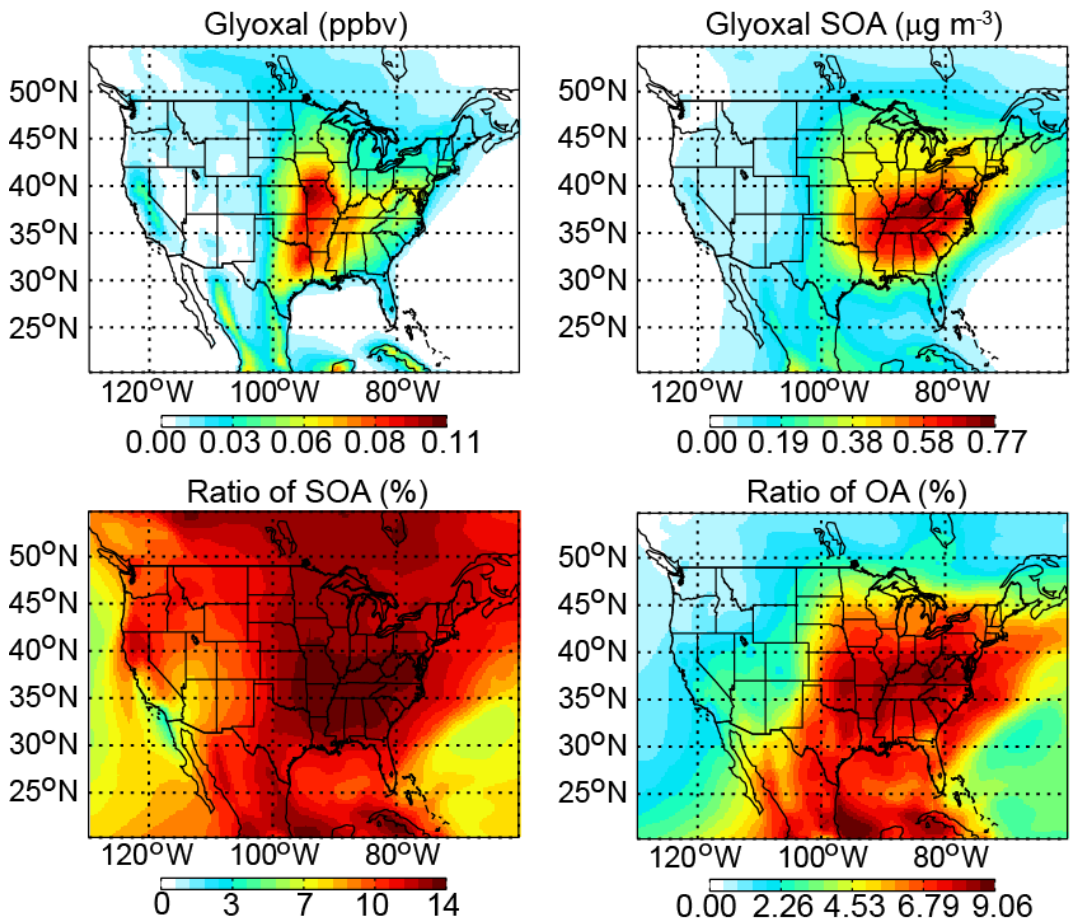

Figure S7. Monthly averaged glyoxal (ppbv), glyoxal SOA μg m^{-3}, ratio of glyoxal SOA to total SOA, and ratio of glyoxal SOA to total organic aerosol (OA) predicted by AM3ST with $\gamma_{glyx}=2.0 \times 10^{-3}$ below 1.5 km.

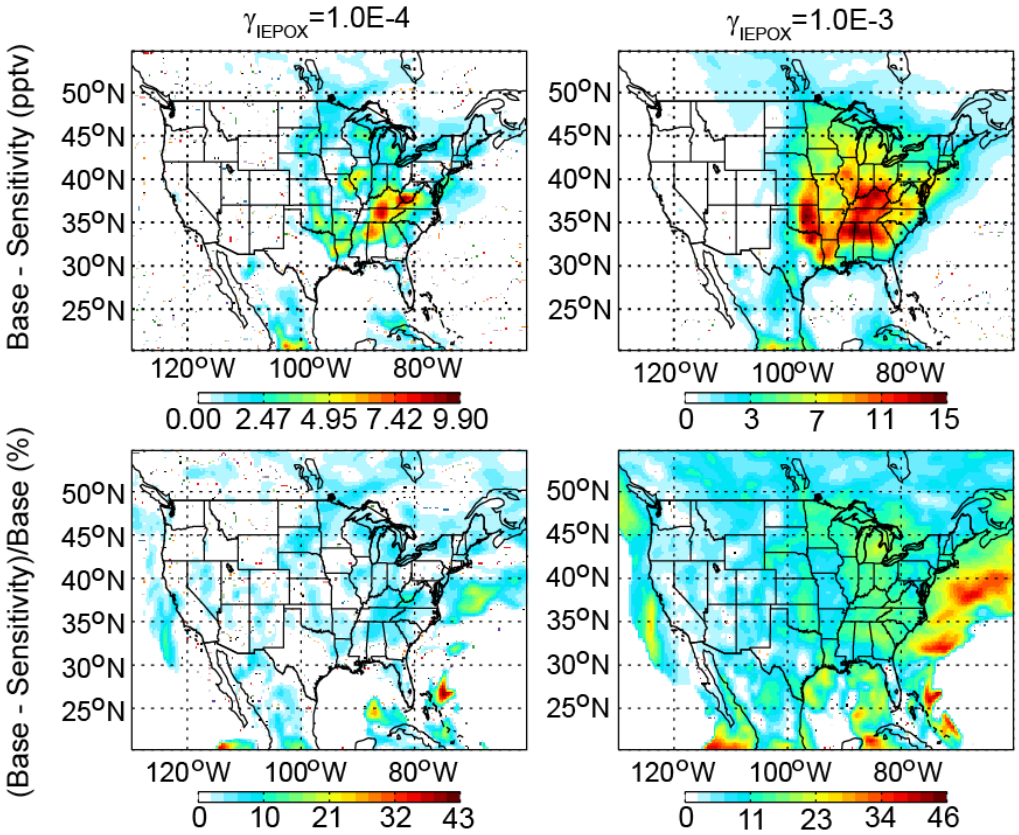

Figure S8. Sensitivity of estimated glyoxal (monthly averaged in the boundary layer) to heterogeneous loss of IEPOX. The Base case is from the AM3B mechanism without heterogeneous loss of glyoxal and IEPOX; sensitivity cases are from the AM3B mechanism without heterogeneous loss of glyoxal but with heterogeneous loss of IEPOX under two conditions (reactive uptake coefficient γ_{IEPOX} are 1.0×10^{-4} (left column) and 1.0×10^{-3} (right column). Absolute difference (pptv) is calculated as base case – sensitivity case (top row); relative difference (%) is calculated as (base case – sensitivity case)/sensitivity case (bottom row).

Table S1. Reaction rates of glyoxal and HCHO in AM3 and MCM v3.3.1 mechanisms. For the calculation of photolysis rates, box model conditions are applied. Units are s^{-1} or molecule^{-1} cm^3 s^{-1}.

Reactions	AM3	MCM v3.3.1
Glyoxal + hν	2.14×10^{-5}	2.87×10^{-5}
Glyoxal + OH	9.70×10^{-12}	9.70×10^{-12}
Glyoxal + NO_3	1.71×10^{-15}	2.73×10^{-15}
HCHO + hν	9.05×10^{-5}	9.05×10^{-5}
HCHO + OH	8.37×10^{-12}	8.49×10^{-12}
HCHO + NO_3	5.79×10^{-16}	5.50×10^{-16}

Table S2. Mean fraction bias (MFB) and mean fraction error (MFE) of glyoxal below 1.5 km. Data from biomass burning, urban plumes, stratospheric air, the Ozark Mountains and flights during nighttime have been excluded[a].

	AM3ST							AM3B				
γ_{glyx} ($\times 10^{-3}$)	0	0.4	0.8	1.2	1.6	2.0	3.0	0	0.1	0.2	0.3	0.4
MFB	0.12	0.23	0.15	0.06	0.07	0.06	-0.08	-0.09	-0.18	-0.19	-0.13	-0.16
MFE	0.62	0.57	0.58	0.59	0.57	0.53	0.61	0.54	0.58	0.61	0.56	0.57

[a]$MFB=\frac{2}{N}\sum_{i=1}^{N}\frac{(P_i-O_i)}{(P_i+O_i)}$, $MFE=\frac{2}{N}\sum_{i=1}^{N}\frac{|P_i-O_i|}{(P_i+O_i)}$, where P_i=prediction, O_i=observation, N=number of data points.